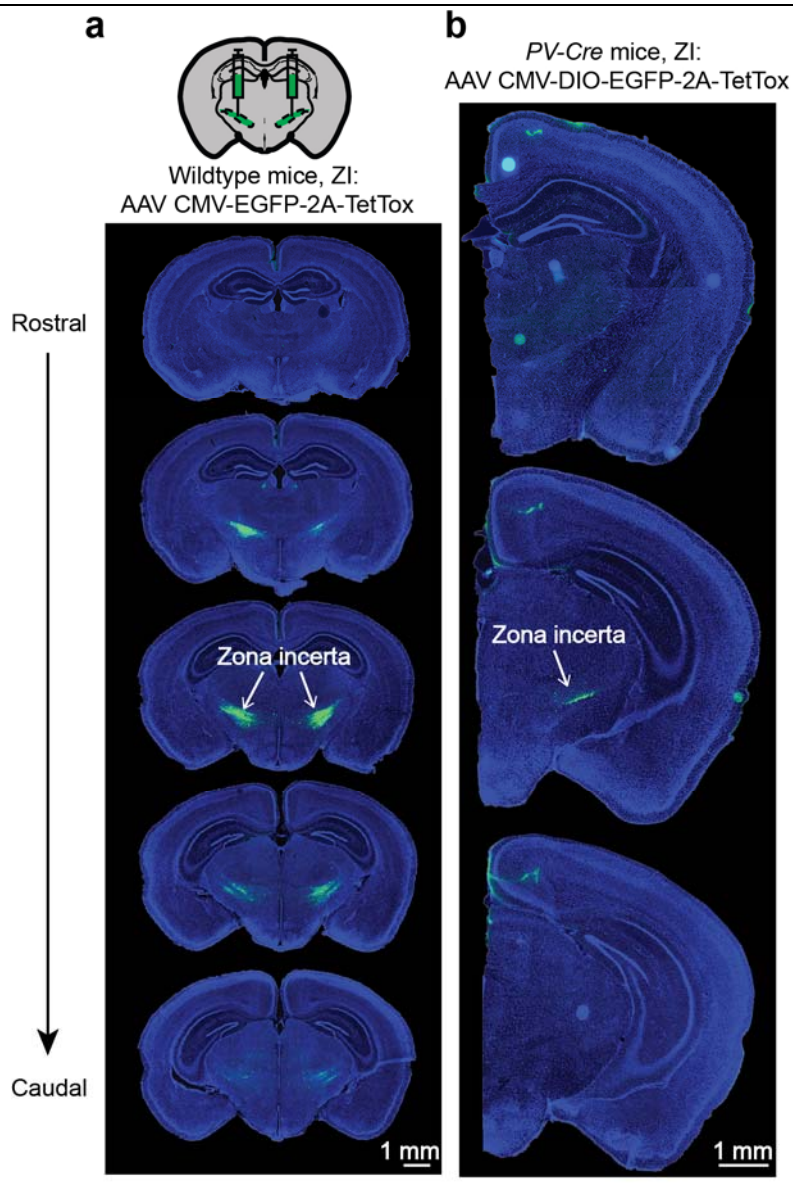

Supplementary Figure 1

Verification of AAV injection sites in the ZI.

(**a**) Top, illustration of bilateral injection of AAV CMV-EGFP-2A-TetTox into ZI. Bottom, representative images of EGFP expression in different brain sections, arranged from rostral to caudal.

(**b**) Sample images of EGFP expression in different brain slices after injection of AAVs expressing double-floxed TetTox and EGFP (CMV-DIO-EGFP-2A-TetTox) into the ZI of *PV-Cre* mice.

Experiments in **a** and **b** were independently replicated with similar results more than ten times.

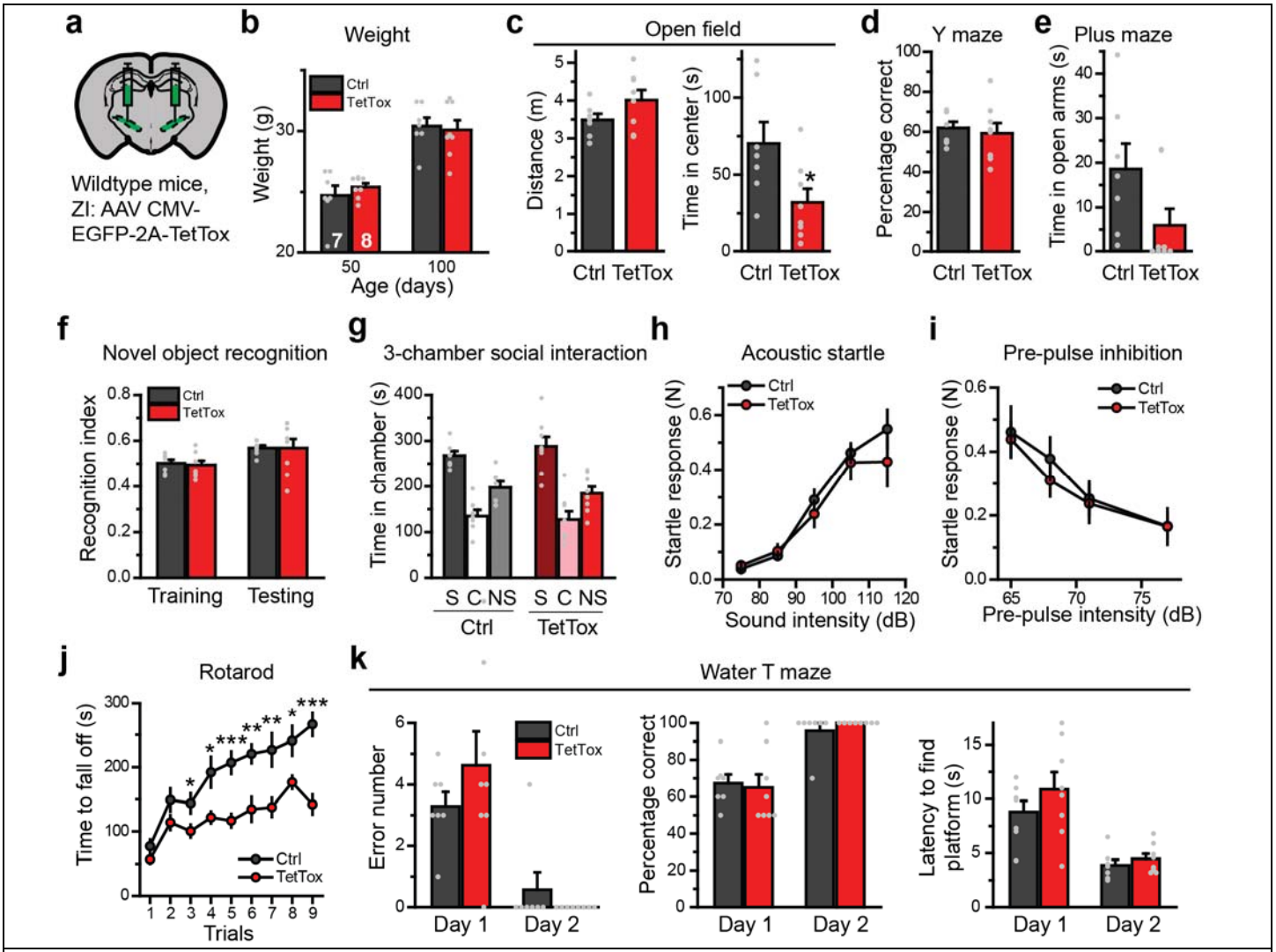

Supplementary Figure 2

Behavioral characterization of mice after inactivation of all synaptic outputs from the medial ZI by expression of TetTox.

(**a**) Illustration of bilateral injections of AAVs expressing TetTox and EGFP (CMV-EGFP-2A-TetTox; test) or only EGFP (CMV-EGFP; control) into the ZI.

(**b**) Body weight of test and control mice at P50 and P100.

(**c**-**k**) Performance of test and control mice in a series of behavioral assays (**c**, open field; **d**, spontaneous alternating Y-maze; **e**, elevated plus maze; **f**, novel object recognition; **g**, three chamber social interaction paradigm; **h**, acoustic startle response; **i**, pre-pulse inhibition; **j**, rotarod; and **k**, water T maze. In **g**, "S" stands for "social", "C" stands for "center" and "NS" stands for "non-social".

Quantitative data are means ± s.e.m.. Statistics were based on two-sided unpaired *t*-tests or Mann-Whitney tests (for datasets that were not normally distributed) for two-group comparisons. $P < 0.05$ was considered significant (*$P < 0.05$, **$P < 0.01$, ***$P < 0.001$). In **c**, $P = 0.13, 0.03$. In **j**, $P = 0.11, 0.11, 0.034, 0.013, 5 \times 10^{-4}, 0.004, 0.009, 0.019, 2 \times 10^{-4}$. n = 7, 8 for control and TetTox injected mice respectively.

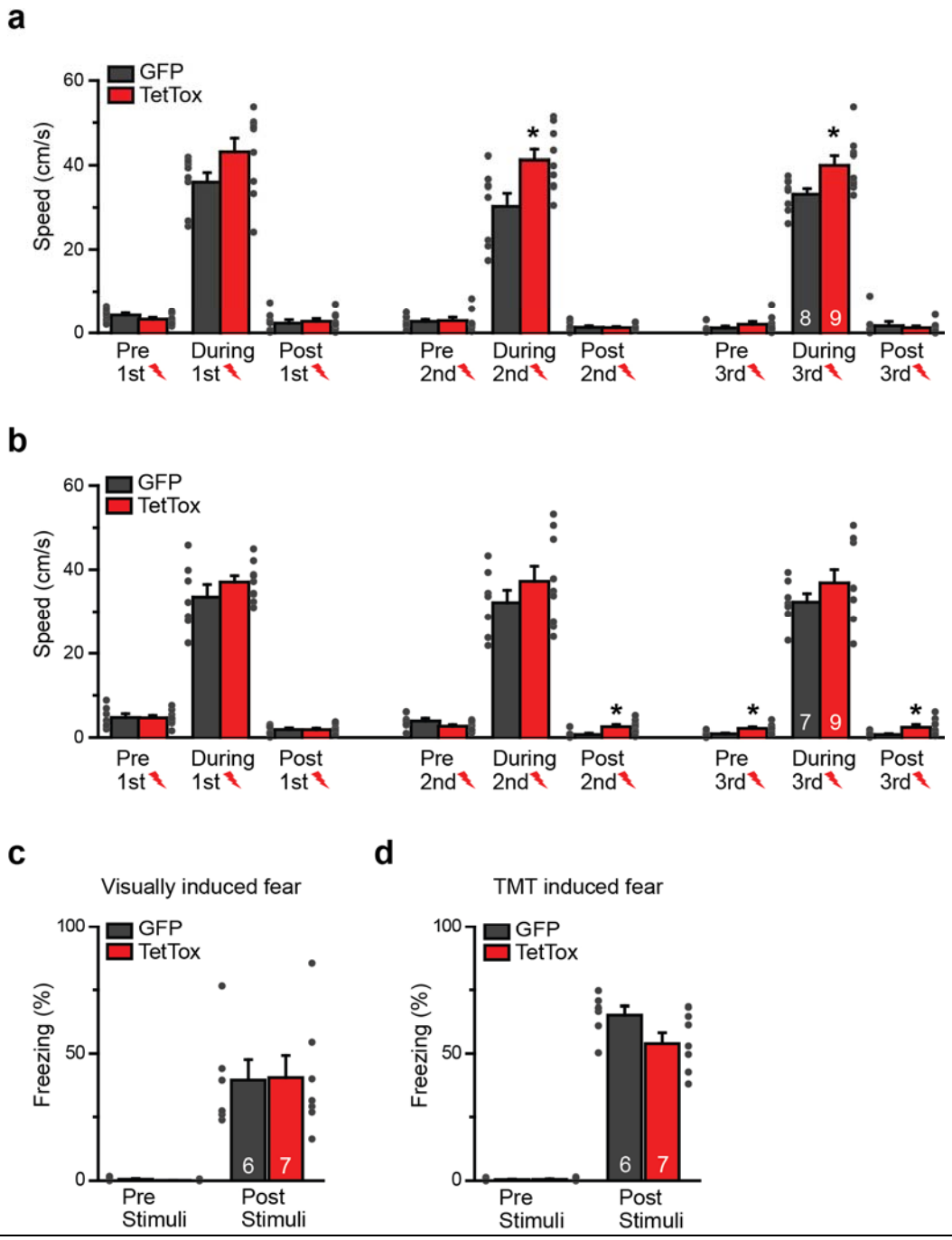

Supplementary Figure 3

Fear memory deficits of ZI TetTox injected mice could not be explained by reduced foot shock responses or freezing expression.

(**a**) Running speed of test and control mice (the same cohort analyzed in **Fig. 1f**) before, during and after delivery of foot shock. *P* = 0.01 (during second foot shock), 0.02 (during third foot shock).

(**b**) Running speed of test and control mice (the same cohort analyzed in **Fig. 1r**) before, during and after delivery of foot shock. *P* = 0.01 (post second foot shock), 0.01 (pre third foot shock), 0.01 (post third foot shock).

(**c**) Freezing percentage of test (DIO-TetTox bilaterally injected in ZI of *PV-Cre* mice) and control mice (DIO-EGFP bilaterally injected in ZI of *PV-Cre* mice) before and after being exposed to sweeping visual stimuli.

(**d**) Freezing percentage of test and control mice (the same cohort used in **c)** before and after being exposed to TMT.

Quantitative data are means ± s.e.m.. Statistics were based on two-sided unpaired *t*-tests or Mann-Whitney tests (for datasets that were not normally distributed) for two-group comparisons. $P < 0.05$ was considered significant (*$P < 0.05$, **$P < 0.01$, ***$P < 0.001$). All numbers of mice used are presented in right bars.

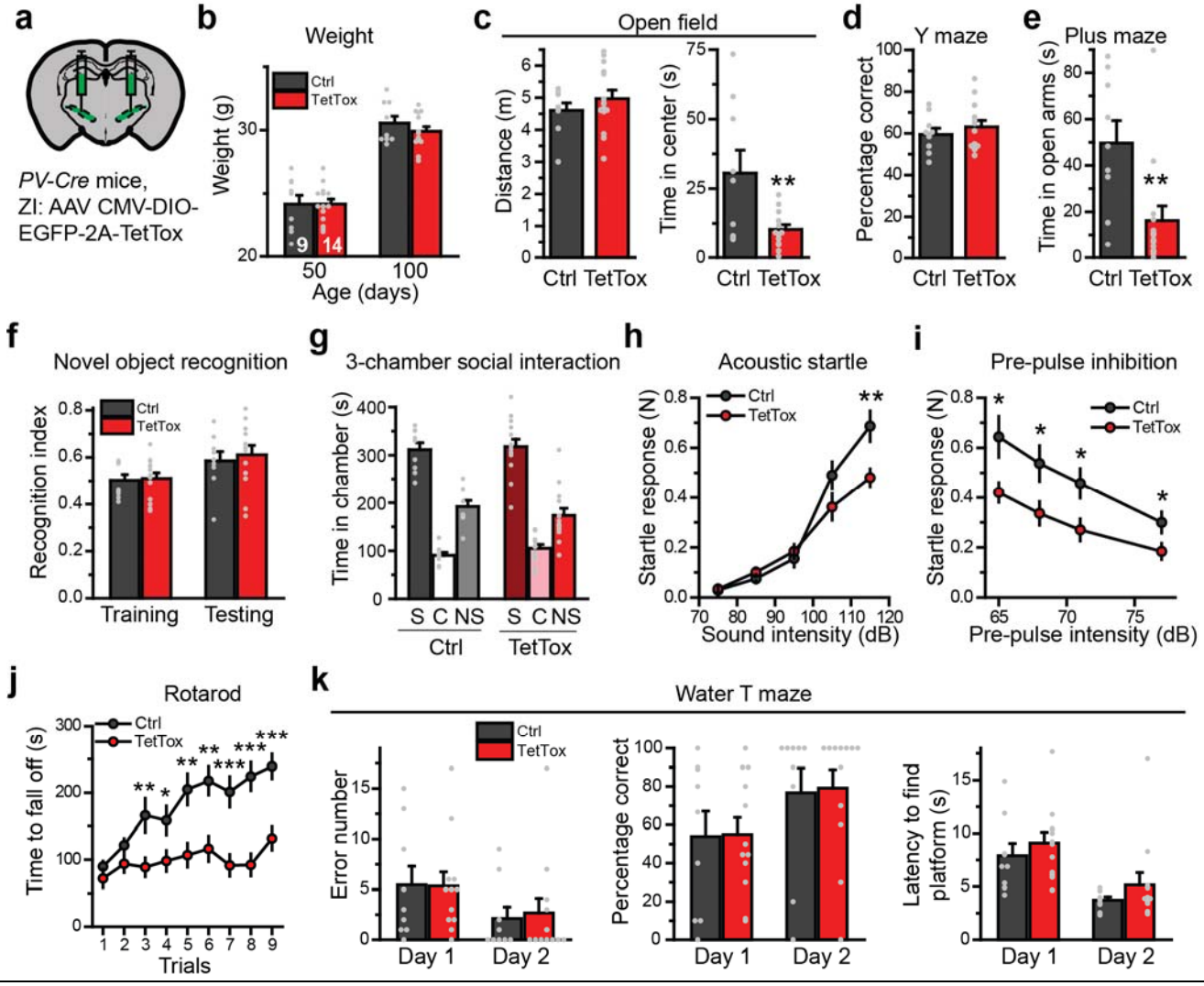

Supplementary Figure 4

Behavioral characterization of mice after inactivation of synaptic outputs from only *PV*$^{+}$-neurons in the ZI.

The panels are arranged for the same experiments as in **Supplementary Figure 2** in the same order, but experiments were performed with mice in which TetTox and EGFP or only EGFP were expressed in *PV*$^{+}$-neurons of the ZI. This was achieved by infecting ZI neurons in *PV-Cre* mice with AAVs containing double-floxed coding regions for TetTox and EGFP or EGFP alone. Note that for the behaviors assayed, the inactivation of all neurons in the ZI or of only *PV*$^{+}$-neurons produced similar impairment patterns.

Quantitative data are means ± s.e.m.. Statistics were based on two-sided unpaired *t*-tests or Mann-Whitney tests (for datasets that were not normally distributed) for two-group comparisons. $P < 0.05$ was considered significant (*$P < 0.05$, **$P < 0.01$, ***$P < 0.001$). In **c**, $P = 0.36, 0.008$. In **e**, $P = 0.006$. In **h**, $P = 0.3, 0.2, 0.5, 0.13, 0.005$. In **i**, $P = 0.013, 0.024, 0.019, 0.041$. In **j**, $P = 0.36, 0.17, 0.009, 0.03, 0.004, 0.003, 7 \times 10^{-4}, 1 \times 10^{-4}, 8 \times 10^{-4}$. n = 9, 14 for control and TetTox injected mice respectively.

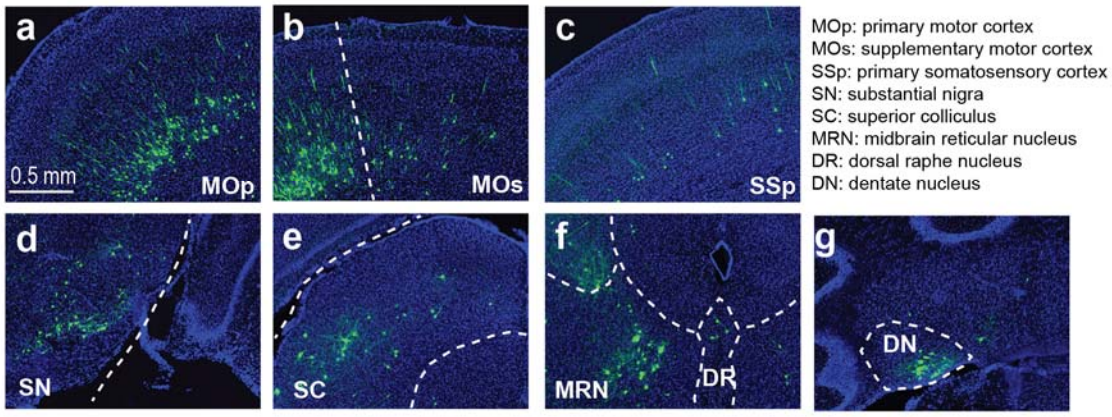

Supplementary Figure 5

Examples of additional brain regions that provide presynaptic inputs to *PV*$^{+}$-neurons in the ZI besides those shown in **Figure 2c**.

Brain regions shown in the panels are labeled by abbreviations that are explained on the top right. Dashed lines indicate approximate boundaries between various brain nuclei. Experiments were independently replicated with similar results five times.

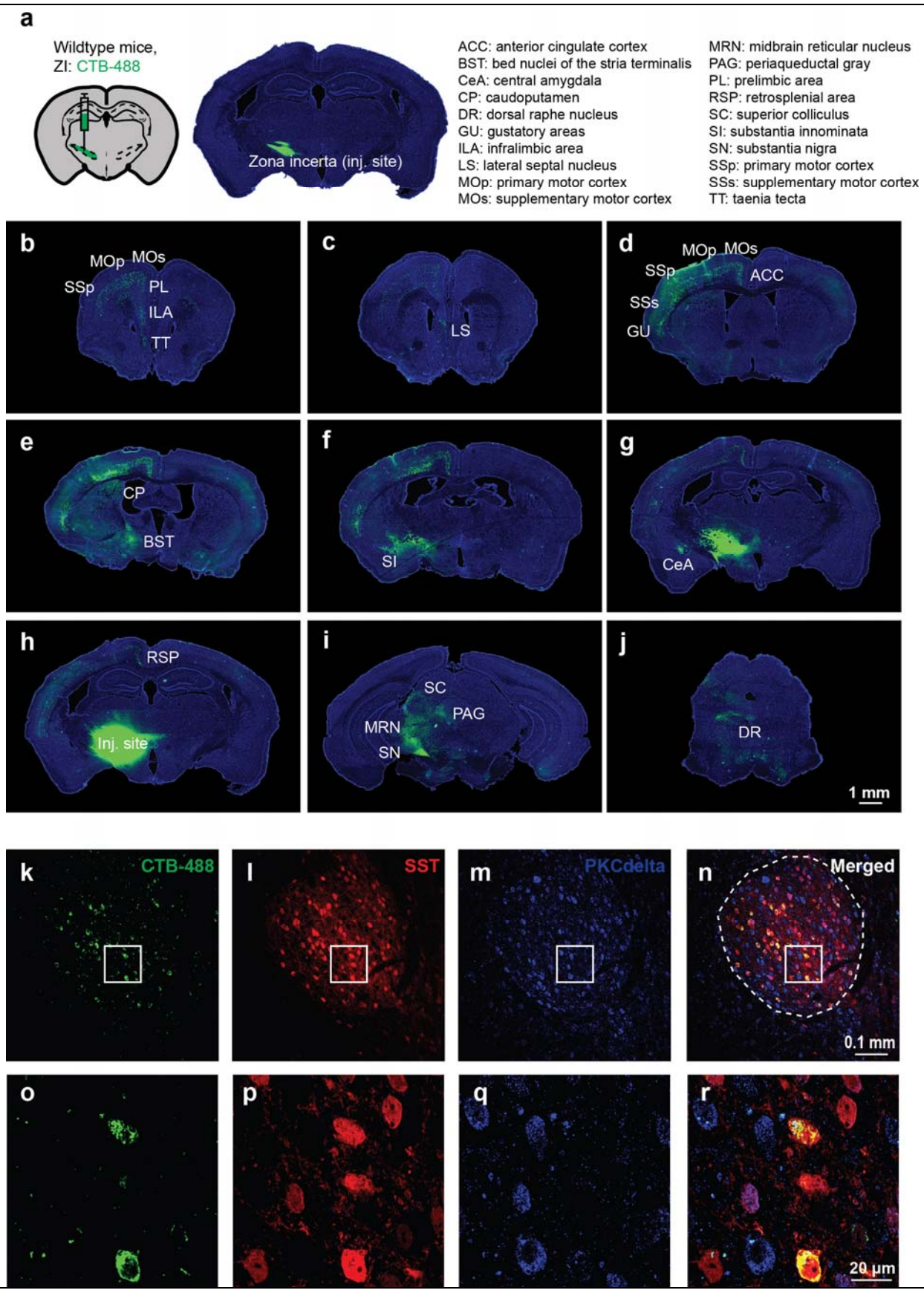
a
Wildtype mice,
ZI: CTB-488
Zona incerta (inj. site)
ACC: anterior cingulate cortex
BST: bed nuclei of the stria terminalis
CeA: central amygdala
CP: caudoputamen
DR: dorsal raphe nucleus
GU: gustatory areas
ILA: infralimbic area
LS: lateral septal nucleus
MOp: primary motor cortex
MOs: supplementary motor cortex
MRN: midbrain reticular nucleus
PAG: periaqueductal gray
PL: prelimbic area
RSP: retrosplenial area
SC: superior colliculus
SI: substantia innominata
SN: substantia nigra
SSp: primary motor cortex
SSs: supplementary motor cortex
TT: taenia tecta
b
MOp
MOs
SSp
PL
ILA
TT
c
LS
d
MOp
MOs
SSp
ACC
SSs
GU
e
CP
BST
f
SI
g
CeA
h
RSP
Inj. site
i
SC
PAG
MRN
SN
j
DR
1 mm
k
CTB-488
l
SST
m
PKCdelta
n
Merged
0.1 mm
o
p
q
r
20 µm

Supplementary Figure 6

Retrograde tracing using Alexa-488 conjugated cholera toxin subunit B (CTB-488) reproduces the presynaptic inputs identified by retrograde rabies tracing in **Figures 2c**, **2d** and **Supplementary Figure 5**, and defines additional inputs that may be targeting non-*PV*$^{+}$-neurons in the ZI.

(**a**) Illustration of the CTB-488 injection into the left ZI (left), and example image showing the injection site (right).

(**b**-**j**) Representative images arranged in a rostral to caudal sequence to display CTB-488 labelled neurons in different brain areas after ZI injections of CTB-488. Please note that the exposures were increased compared to **a** to reveal presynaptic neurons. As a result, there are strong false positive signals around injection site in **g**-**i.** Abbreviations used in the various panels are explained on the top right.

(**k**-**n**) Representative images illustrating the co-localization of CTB retrogradely labelled CeA neurons with *SST*$^{+}$- and *PKCdelta*$^{+}$-neurons. The same injection scheme was used as in **a**, except that *SST-Ai14* mice were used. *PKCdelta*$^{+}$-neurons were recognized by antibody staining.

(**o**-**r**) Enlarged images of the boxed area shown in **k**-**n**.

Experiments in **a**-**j** and **k**-**r** were independently repeated with similar results four and three times, respectively.

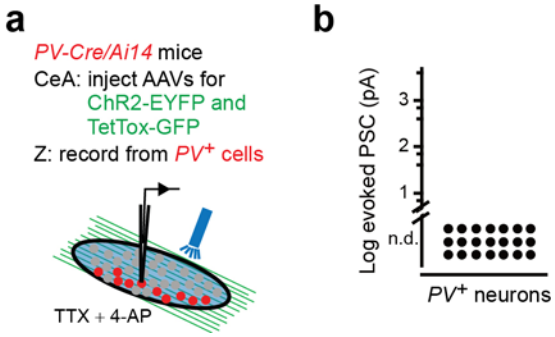

Supplementary Figure 7

TetTox blocks synaptic transmission from CeA to ZI *PV*$^{+}$-neurons.

(**a**) Experimental strategy with channelrhodopsin (ChR2-EYFP) and TetTox (TetTox-GFP) co-expression in the CeA of *PV-Cre/Ai14* mice. Postsynaptic currents recorded from *PV*$^{+}$-neurons were evoked by optogenetic stimulation in the presence of TTX and 4-AP.

(**b**) Synaptic response amplitude plot. n = 21 recorded *PV*$^{+}$-neurons. n.d.: not detected.

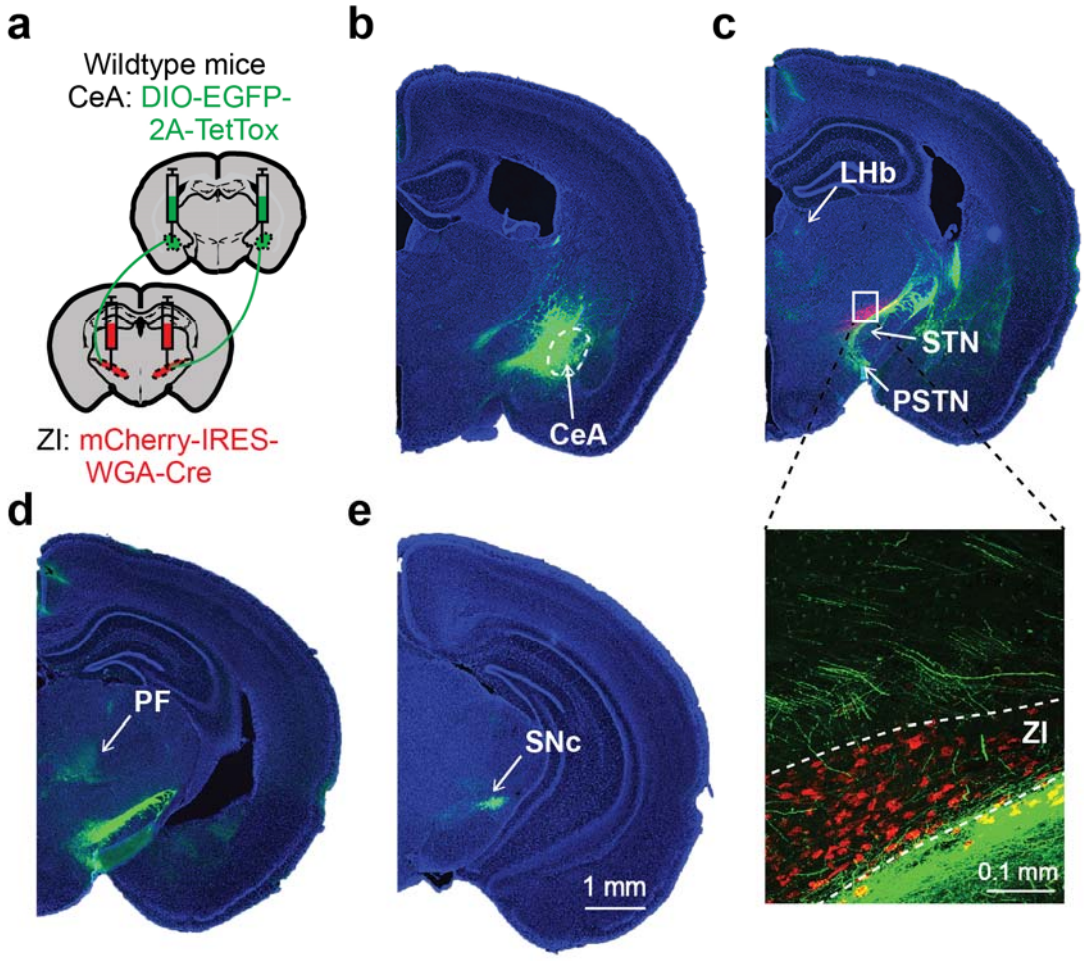

Supplementary Figure 8

Verification of injection sites for AAVs expressing WGA-Cre in the ZI and TetTox-EGFP in the CeA.

(a) Experimental strategy.

(**b**) Representative image showing the expression of EGFP in CeA.

(**c**) Top, representative image showing the expression of mCherry and WGA-Cre in the ZI and the green axons from CeA neurons that innervate the ZI. Bottom, enlarged confocal image showing the boxed area. The ZI area was delineated by white dashed lines. LHb, lateral habenula; STN, subthalamic nucleus; PSTN, parasubthalamic nucleus.

(**d**-**e**) Different sections illustrating the collateral projections of CeA-ZI pathway. PF, parafascicular nucleus; SNc, substantia nigra compact part.

Experiments were independently repeated with similar results more than ten times. Note that WGA-Cre 'starter cells' (i.e., the initially infected cells) are red owing to co-expressed mCherry; WGA-Cre mediates retrograde trans-synaptic transfer of Cre to presynaptic inputs, but not of mCherry, and thus input cells are not red. Input cells in CeA, however, are green because the retrogradely transported Cre activates the double floxed TetTox-2A-EGFP expression, thereby silencing CeA-ZI projections. CeA-ZI pathway also have other collateral projections (labelled by arrows).

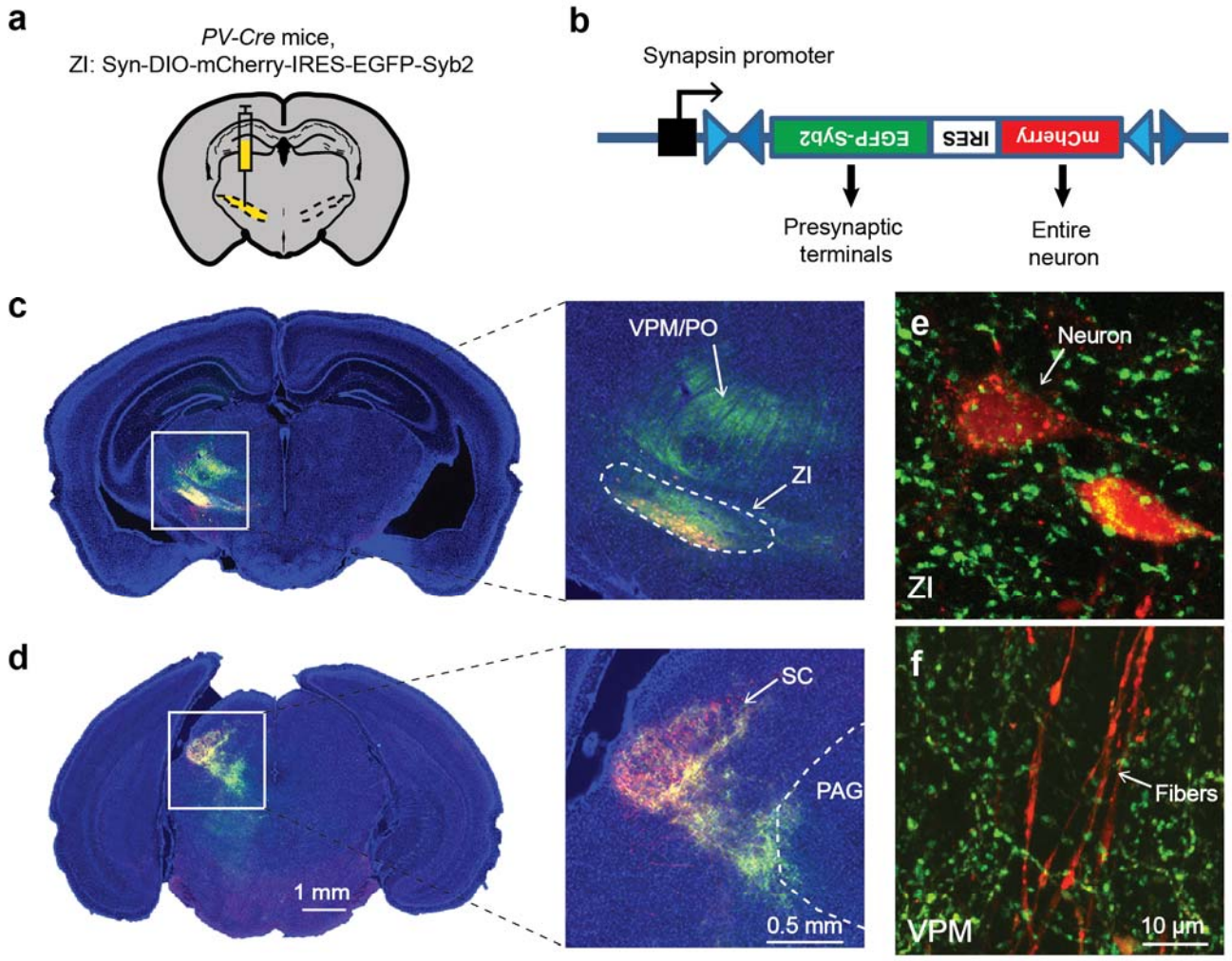

Supplementary Figure 9

SynaptoTag tracing of efferent targets of ZI *PV*$^{+}$-neurons identifies neurons in thalamic regions, the superior colliculus, the periaqueductal gray and the ZI itself as postsynaptic targets of ZI *PV*$^{+}$-neurons.

(**a**) Illustration of the injection of AAVs expressing double-floxed SynaptoTag (DIO-SynaptoTag) into the left ZI of *PV-Cre* mice.

(**b**) Schematic of the DIO-SynaptoTag construct.

(**c**) Representative images showing the AAV injection site in the ZI and presynaptic terminals formed by ZI *PV*$^{+}$-neurons in the thalamus (left overview; right, enlarged area from the boxed region in the overview). Note that in the enlarged image the red fluorescence intensity was lowered to reveal the location of infected neurons in ventral ZI. Green fluorescence, representing presynaptic terminals, could be observed in ZI itself and in the ventral posteromedial thalamic nucleus (VPM) and the posterior complex of the thalamus (PO).

(**d**) Representative images showing strong presynaptic SynaptoTag signals in the superior colliculus (SC) and the periaqueductal gray (PAG) of the midbrain (left overview; right, enlarged area from the boxed region in the overview). Note that the presynaptic terminals

are located in the lateral and deeper layer of the SC, as well as in the lateral part of PAG.

(**e**, **f**) High magnification images showing the red fluorescence in the cell body and axon fibers and the green fluorescence in presynaptic terminals in the ZI (**e**) and the VPM (**f**).

Experiments were independently repeated with similar results three times.

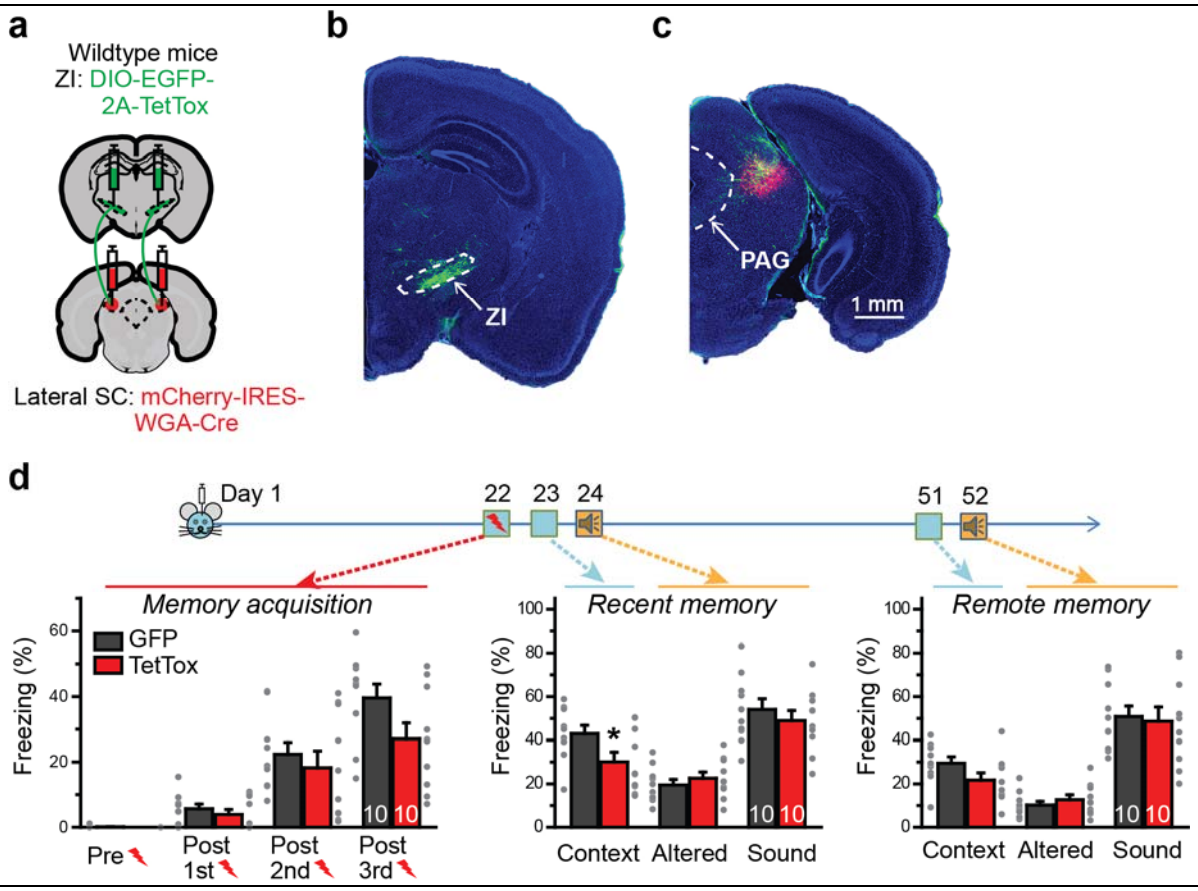

Supplementary Figure 10

Silencing medial ZI─lateral SC pathway does not replicate the fear memory deficits observed in ZI TetTox injected mice.

(a) Stereotaxic viral injection strategy.

(**b**) Representative image showing the expression of EGFP in medial ZI.

(**c**) Representative image showing the expression of mCherry and WGA-Cre in the lateral SC and the green axons from ZI neurons that innervate the lateral SC. Note that mCherry signal is in the lateral SC without spreading to PAG, and EGFP$^+$-neurons are restricted to the ventral ZI, where *PV*$^+$-neurons are supposed to be located. Imaging experiments were independently repeated with similar results five times.

(**d**) Tests of memory acquisition, recent memory and remote memory after blocking medial ZI-lateral SC pathway. Quantitative data are means ± s.e.m.. Statistics were based on two-sided unpaired *t*-tests or Mann-Whitney tests (for datasets that were not normally distributed). $P = 0.043$ for the comparison of contextual recent memory. n = 10, 10 for control and TetTox injected mice respectively. Note that the same cohort of mice were used for recent and remote fear memory test.

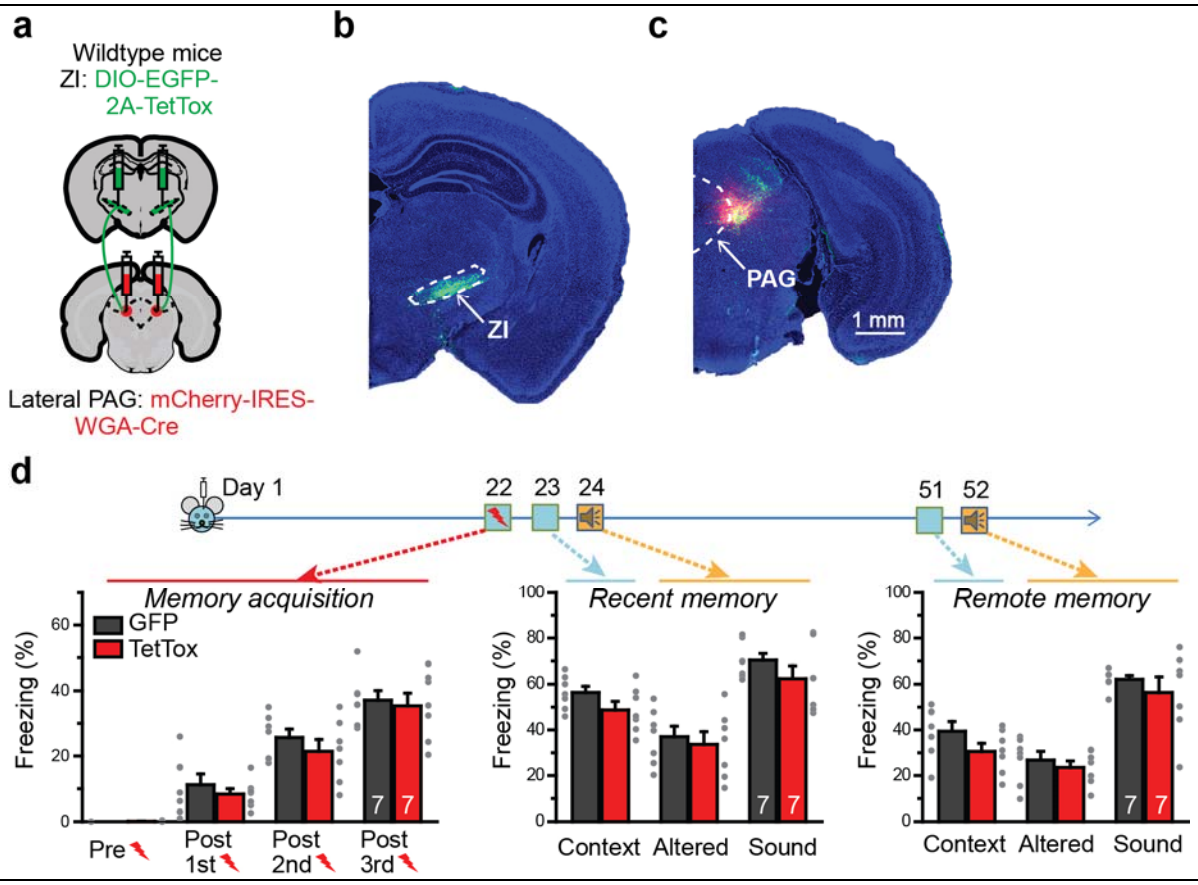

Supplementary Figure 11

Silencing medial ZI–lateral PAG pathway does not replicate the fear memory deficits observed in ZI TetTox injected mice.

(**a**-**d**) The panels are arranged for the same experiments as in **Supplementary Figure 10** in the same order, but experiments were performed with WGA-Cre and mCherry expressed in the lateral PAG. Representative images in **b**-**c** were independently repeated with similar results five times. Quantitative data are means ± s.e.m.. Statistics were based on two-sided unpaired *t*-tests or Mann-Whitney tests (for datasets that were not normally distributed). $P < 0.05$ was considered significant. n = 7, 7 for control and TetTox injected mice respectively. Note that the same cohort of mice were used for recent and remote fear memory test.

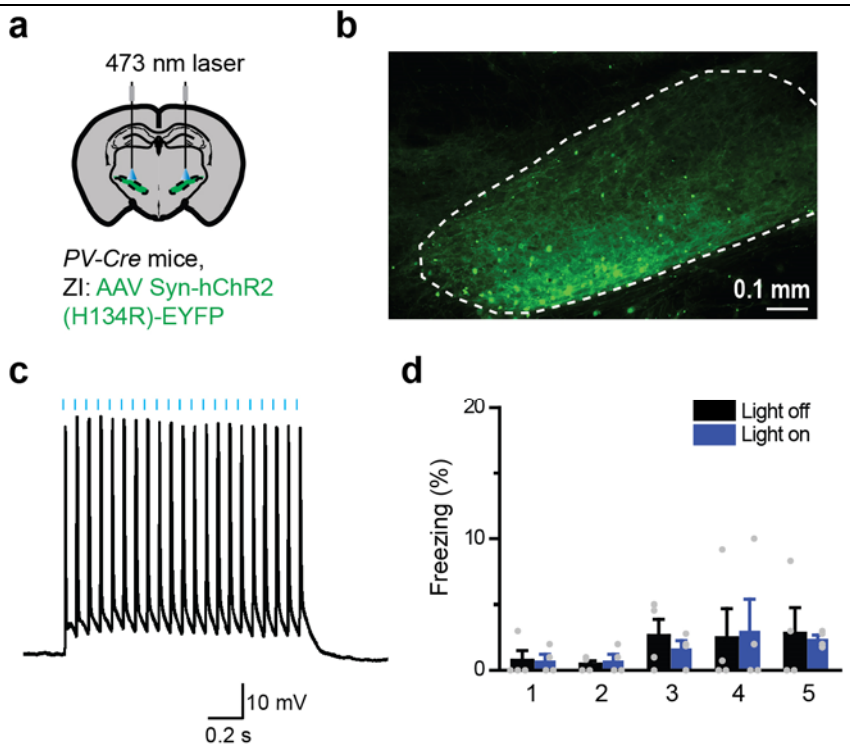

Supplementary Figure 12

Optogenetically activating ZI *PV*$^{+}$-neurons does not directly drive freezing behavior.

(**a**) Stereotaxic viral injection and optic fiber implantation strategy.

(**b**) Representative image showing the expression of ChR2 in the ZI. Experiments were independently repeated with similar results three times.

(**c**) Representative trace of membrane potential change in response to a 15 Hz train of blue laser stimulation.

(**d**) Summary of animals' freezing behavior in response to five repeats of 15 Hz light stimulation (see **methods**). Statistics were based on two-sided paired *t*-tests or Mann-Whitney tests (for datasets that were not normally distributed). $P < 0.05$ was considered significant. n = 4 mice. Different stimulation frequencies were tested and none of them were found to drive freezing (data not shown).